IEEE Access
Multidisciplinary ⋮ Rapid Review ⋮ Open Access Journal

Received 27 March 2023, accepted 25 April 2023, date of publication 27 April 2023,
date of current version 8 December 2023.

Digital Object Identifier 10.1109/ACCESS.2023.3271122

RESEARCH ARTICLE

Estimation and Validation of Land Surface Temperature Using Chinese Geostationary FengYun Meteorological Satellite (FY-2D) Data in an Arid Region

XIN PAN, SUYI LIU, ZI YANG, XI ZHU, YINGBAO YANG, WENYING XIE, JIE YUAN, ZHANCHUAN WANG, AND HAO SONG

School of Earth Science and Engineering, Hohai University, Nanjing 211100, China
Jiangsu Province Engineering Research Centre of Water Resources and Environment Assessment Using Remote Sensing, Hohai University, Nanjing 211100, China

Corresponding author: Yingbao Yang (yyb@hhu.edu.cn)

This work was supported in part by the National Natural Science Foundation of China under Grant 42230112, Grant 41701487, Grant 42071346 and Grant 42371397; in part by the Fundamental Research Funds for the Central Universities of China under Grant 2019B02714; and in part by the State Scholarship Fund of China.

ABSTRACT This study calibrated a refined split-window algorithm for land surface temperature (LST) retrieval based on Fengyun-2D (FY-2D) meteorological satellite. First, FY-2D land surface emissivity (LSE) was predicted from Moderate-resolution Imaging Spectroradiometer (MODIS) LSE based on sensors spectral similarities. The retrieved FY-2D LST data were validated in an arid region where the traditional split-window algorithm generally performed unsatisfactorily. Validation results show R^2 (coefficient of determination) and RMSE (root mean square error) values range 0.53–0.67 and 2.86–6.21 K, respectively, against ground observed LST. Better LST retrievals were observed over vegetated regions with an RMSE value of ∼2.8 K. Spatially, the FY-2D LST was highly correlated ($R^2 = 0.83$) with and showed marginal differences (±2 K) from MODIS LST for ∼40% of the whole area.

INDEX TERMS Calibration and validation, FY-2D, land surface temperature, refined split-window algorithm.

I. INTRODUCTION

As an important component of water and energy budget for surface, land surface temperature (LST) is a key parameter for the meteorology, hydrology, ecology and urban climate [1], [2], [3]. Owning to the development of remote sensing, LST can be obtained at a large spatio-temporal scale in the way of various algorithms, such as single-channel methods, split-window algorithms, land surface temperature and emissivity separation methods [4], [5], [6], [7], [8].

As the algorithm used in the production of moderate-resolution imaging spectroradiometer (MODIS) LST product, split-window algorithms were most widely used to retrieve LST based on the differential water vapor absorption in two adjacent infrared channels since the McMillin's estimation attempt [9].

To improve the applicability of split-window algorithm, Wan improve his split-window algorithm, called refined split-window algorithm, to obtain the MODIS LST product of V6.3.0 [6], [7]. The accuracy of V6.3.0 LST was significantly better than that of V5 with the errors decrease from 2 K to less than 1 K at some bare soil sites. Similarly, this algorithm was also used to retrieve LST using other polar-orbit satellite data (e.g. AVHRR, GF-5), and improve the performance of split-windows [10], [11], [12].

Relative to the widely used polar-orbit satellites, geostationary satellites can obtain various images in a day for a certain region, which is beneficial for understanding water and energy budgets [13]. Therefore, several researchers retrieved LST using geostationary satellites such as Meteosat Second

The associate editor coordinating the review of this manuscript and approving it for publication was Turgay Celik.

Generation (MSG), Geostationary Operational Environmental Satellite (GEOS) Himawari and Fengyun [14], [15], [16], [17], [18], [19]. Considering that Fengyun is almost the only satellite to derive the continual diurnal and regional LST in China, especially in the western of China, some researchers applied the split-window algorithm to LST retrieval in China using Fengyun satellite. Tang initially retrieved LST from FengYun-2C (FY-2C) data using the split-window algorithm of Wan and Dozier [6], [20]. Zhang and Wang subsequently retrieved LST from FY-2D data based on a split-window algorithm with a correlation coefficient of 0.5 and a root mean square error (RMSE) of 4.4 K between the retrieval and the MODIS product [21]. Song et al. also used FY-2E data and split-window algorithm of Wan and Dozier to retrieve LST of source region of the Yellow River with a correlation coefficient (R) varying from 0.60 to 0.94 and a root mean square error ranging from 1.89 to 3.71 K between retrieved and MODIS LST [22]. Worth noting, those studies were focused on the LST retrieval of FY-2 in the vegetated region using the previous split-window algorithm of Wan and Dozier [6].

For split-window algorithm of Wan, the coefficient and lookup table are different for each sensor. The coefficient and lookup table of refined split-window algorithm are not simulated for FY-2. Considered that the long time series of FY-2 and the successful application of refined split-window algorithm in Himawari-8 [18], it is valuable to regress the coefficient and build lookup table for the refined split-window algorithm for FY-2D, and apply the refined split-window algorithm of Wan to LST retrieval of FY-2D data in a region [7]. Section II presents information regarding the study area and data gathered. The Section III describes the algorithm of Wan and simulates the numerical values of the coefficients in that algorithm for FY-2D. Section IV performs the result of LST retrieval, and evaluates the results. Section V discusses the reason of the difference of retrieval and MODIS LST. Section VI concludes the paper.

II. STUDY AREA AND DATA

A. STUDY AREA

The study areas are located in a part of Zhangye city which is an oasis-desert ecotone (31°14′ –32°37′N, 118°22′ –119°14′E) within the middle reaches of Heihe Basin in Northwest China. The area experiences an arid continental climate with the annual mean temperature and precipitation with values of 280.5 K and 115.6 mm, respectively [23]. There are three main land cover types, namely, wetland, vegetation and desert, which are located in the north, middle, and northwest (southeast, southwest) parts, respectively. Four ground sites (wetland, crop, desert1 and desert2 sites) were chosen (Figure 1), including two vegetated sites (wetland and crop sites) and two desert sites (desert1 and desert2 sites), which are belong to the Heihe Watershed Allied Telemetry Experimental Research (HiWATER). All ground observation data were provided by the Cold and Arid Regions Science Data Center at Lanzhou [24], [25]. With field observations, the homogeneity around sites is relatively good within the scope of 5km.

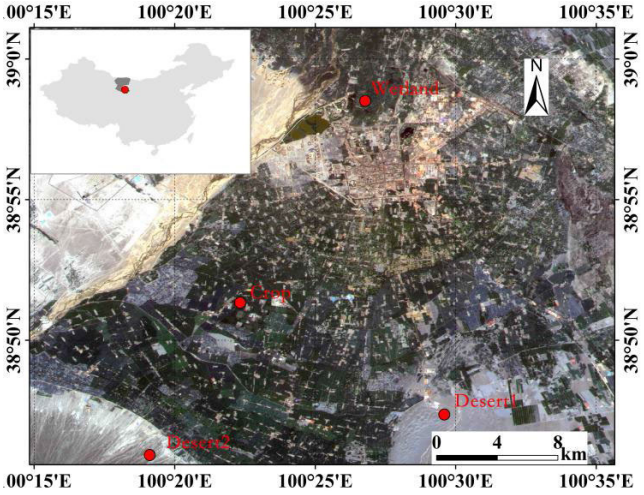

FIGURE 1. Sites and underlying surfaces of the study in Zhangye city.

B. DATA DESCRIPTION

The data used for LST estimation were obtained from FY-2D data and MODIS product. FY-2D which can obtain one full disc image covering the area of 80° N-80° S and 26.5°E-146.5°E is one of five geostationary meteorological satellites of China, namely, FY-2C/2D/2E/2F/2G [26]. The upgraded Stretched-Visible and Infrared Spin-Scan Radiometer (S-VISSR) onboard on FY-2D include one visible channel and four infrared channels. The FY-2D satellite data in two thermal infrared channels (IR1, 10.3-11.3 μm and IR2, 11.5-12.5 μm) which can be used in the spilt-window algorithm, were provided by China Meteorological Administration (CMA). The spatio-temporal resolution of FY-2D in IR1 and IR2 is 5km and 30min [27]. All selected images (11 images) were acquired from June 20, 2012 to July 20, 2012.

MODIS products were provided by the Level 1 and Atmosphere Archive and Distribution System (LAADS) of the National Aeronautics and Space Administration (NASA) [28]. In our study, MOD11 was selected to obtain LST and land surface emissivity (LSE) in temporal-spatial resolution of 1 day and 1 km. The temporal and spatial resolutions of these products are listed in Table 1.

TABLE 1. Available datasets in our study.

Datasets	Sources	Parameters	Resolutions	Usage
FY-2D	CMA	Brightness	30min，5km	Retrieval of LST
MOD11_L2	NASA	LST	5min，1km	Validation
MOD11_A1	NASA	LSE	5min，1km	Estimation of LSE
TIGR2002	LMD	Profiles of atmosphere	-	Coefficient calibration
Ground Measurement	HiWATER	Longwave Radiation	10min	Validation

Accordingly, the ground observations spanning from June 20, 2012 to July 20, 2012 were also provided by the Cold and Arid Regions Science Data Center at Lanzhou [24]. They were used for validation. The LST reference is estimated from the upwelling and downwelling longwave radiation measured by pyranometers/pyrgeometers using this equation [29]:

$$T_s = \left[\frac{R_{lu} - (1-\varepsilon_b)\cdot R_{ld}}{\varepsilon_b \cdot \sigma}\right]^{1/4} \tag{1}$$

where R_{lu} (R_{ld}) is the surface upwelling (downwell) longwave radiation, σ is the Stefan–Boltzmann's constant, ε_b is the broadband LSE [30], [31].

III. METHODS

A. REFINED SPLIT-WINDOW ALGORITHM

Based on refined split-window algorithm proposed by Wan, LST can be expressed as [6]

$$\begin{aligned} LST = {} & b_0 + \left(b_1 + b_2\frac{1-\varepsilon}{\varepsilon} + b_3\frac{\delta\varepsilon}{\varepsilon^2}\right)\frac{T_{IR1}+T_{IR2}}{2} \\ & + \left(b_4 + b_5\frac{1-\varepsilon}{\varepsilon} + b_6\frac{\delta\varepsilon}{\varepsilon^2}\right)\frac{T_{IR1}-T_{IR2}}{2} \\ & + b_7\,(T_{IR1}-T_{IR2})^2 \end{aligned} \tag{2}$$

where ε and $\delta\varepsilon$ are the mean and difference of LSE in band 31 and 32 of MODIS, TIR1 and TIR2 are the top of atmosphere (TOA) brightness temperature in band 31 and 32 of MODIS, respectively. b_1 - b_7 are the unknown coefficients which will be derived in the following from simulated FY-2D data.

Then, atmospheric radiative transfer simulations were made with MODTRAN4 code in wide atmospheric and LST conditions using the 1413 selected data (in clear sky) of Thermodynamic Initial Guess Retrieval (TIGR) database TIGR2002 which represents a worldwide set of atmospheric situations (2311 radio soundings) from polar to tropical atmosphere [32], [33].In detail, considering that the reasonable variations of LST are varied in a wide range according to the atmospheric temperature T0 in the first boundary layer of the atmospheric profiles used, the LST in the simulation for each profile was changed between T0 + 5 K and T0 + 30 K at intervals of 5 K [34]. Moreover, considering the most land covers, the averaged emissivity ε was divided into two types, ε varying from 0.90 to 0.96 in a step of 0.1 and ε varying from 0.94 to 0.99 in a step of 0.1, and the emissivity difference $\Delta\varepsilon$ from -0.025 to 0.015 with a step of 0.005, were used in our simulation. In addition, WVC was divided into six subranges with an overlapping range of 0.5 g/cm^2: [0–1.5], [1–2.5], [2–3.5], [3–4.5], [4–5.5], [5–6.5]. Six view zenith angles (VZAs) were considered: 0°, 33.56°, 44.42°, 51.32°, 51.2°, 56.25° and 60°. Subsequently, with atmospheric parameters (atmospheric transmittance, upwelling radiance, and downwelling radiance), LSTs, and emissivities as inputs, the brightness temperature of the top-of-atmosphere (TOA) in the two TIR bands were obtained. Finally, the algorithm coefficients in Equation (2) were obtained using multiple linear regressions.

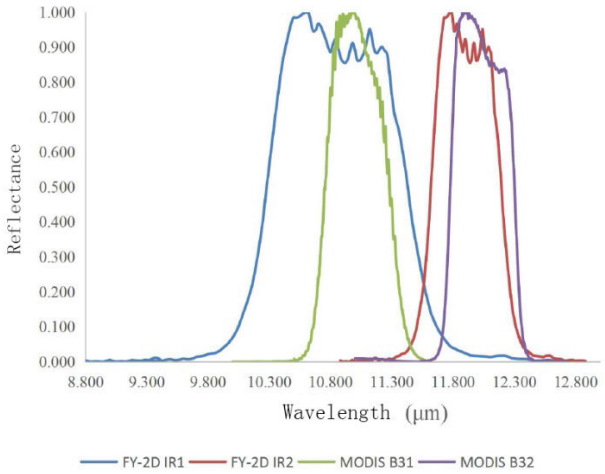

FIGURE 2. Spectral response functions of IR1 and IR2 channels of FY-2D and those of channels 31 and 32 in MODIS.

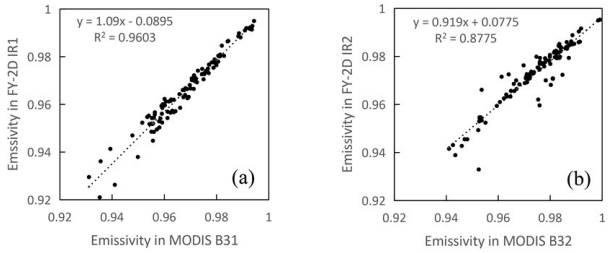

FIGURE 3. Statistical relationship of the emissivities between the FY-2D channels IR1 and IR2 and the MODIS channels 31 (a) and 32 (b), respectively.

In the split-window algorithm, the LSE and WVC are the two key parameters, then we simulate these two parameters in the following.

B. DETERMINATION OF LSEs

Based on the relationships of spectral response functions between IR1 of FY-2D and band 31 of MODIS, IR2 of FY-2D and band 32 of MODIS, the LSEs in bands IR1 and IR2 of FY-2D can be estimated from the LSEs in bands 31 and 32 of MODIS provided by the MODIS LST product. The emissivities in the two split-window bands of MODIS and FY-2D can be calculated using the integrals of the spectral emissivity with the channel response functions, as shown in Figure 2, over the spectral range of the bands. Therefore, the statistical relationships of (3) and (4) between MODIS bands and FY-2D bands are established by a linear regression analysis as shown in Figure 3

$$\varepsilon_{IR1} = 1.09 \times \varepsilon_{b31} - 0.0895 \tag{3}$$

$$\varepsilon_{IR2} = 0.919 \times \varepsilon_{b32} + 0.0775 \tag{4}$$

where ε_{IR1} and ε_{IR2} are LSE in IR1 and IR2 of FY-2D, and ε_{b31} and ε_{b32} are LSE in band 31 and 32 of MODIS

C. DETERMINATION OF ATMOSPHERIC WVC

The atmospheric WVC can be derived from the transmittance ratio of the split-window bands [20], [35]. Considering that the transmittance ratio of the split-window bands is related to the emissivity ratio of the split-window bands, then WVC can be simulated as:

$$WVC = C_1 + C_2 \frac{\varepsilon_{IR1}}{\varepsilon_{IR2}} \frac{\sum_{K=1}^{N} \left(T_{IR1,k} - \overline{T}_{IR1}\right)\left(T_{IR2,k} - \overline{T}_{IR2}\right)}{\sum_{K=1}^{N} \left(T_{IR1,k} - \overline{T}_{IR1}\right)^2} \tag{5}$$

where C_1 and C_2 are the coefficients determined in Tang's research [20], the subscript k denotes pixel k, $T_{IR1,k}$ and $T_{IR2,k}$ are the TOA brightness temperatures measured in bands IR1 and IR2 of the k pixel, and $\overline{T}_{IR1}$ and $\overline{T}_{IR2}$ are the TOA mean channel brightness temperatures of the N neighboring pixels of bands IR1 and IR2, respectively.

D. ASSESSMENT INDICATORS

In this paper, the mean error (bias) was used to evaluate the system error of the model, the root mean square error (RMSE) was used to reflect the sampling standard deviation between the retrieval value and the true value. The consistency index describes the consistency between the retrieval value and the true value, and is often evaluated by liner fitting. In this paper, the coefficient of determination (R^2) is used as the evaluation index.

IV. RESULTS

A. SENSITIVITY ANALYSIS OF LSE AND WVC

Based on the approach of sensitivity analysis [30], [36], [37], the influence of MODIS_LSE on FY-2D_LSE and the influence of FY-2D_LSE on WVC were analyzed, respectively in Figure 4. With the error value of ± 0.01 for MODIS LSE, the error estimates of FY-2D_LSE was within ±0.015, as shown in Figure 4a. In addition, when the ε_{IR1} and ε_{IR2} errors are [−0.01,0.01], the WVC errors are less than ±0.1g/cm2 and ±0.15g/cm2, respectively. This indicates that ε_{IR2} is more sensitive to WVC estimation, as shown in Figure 1b.

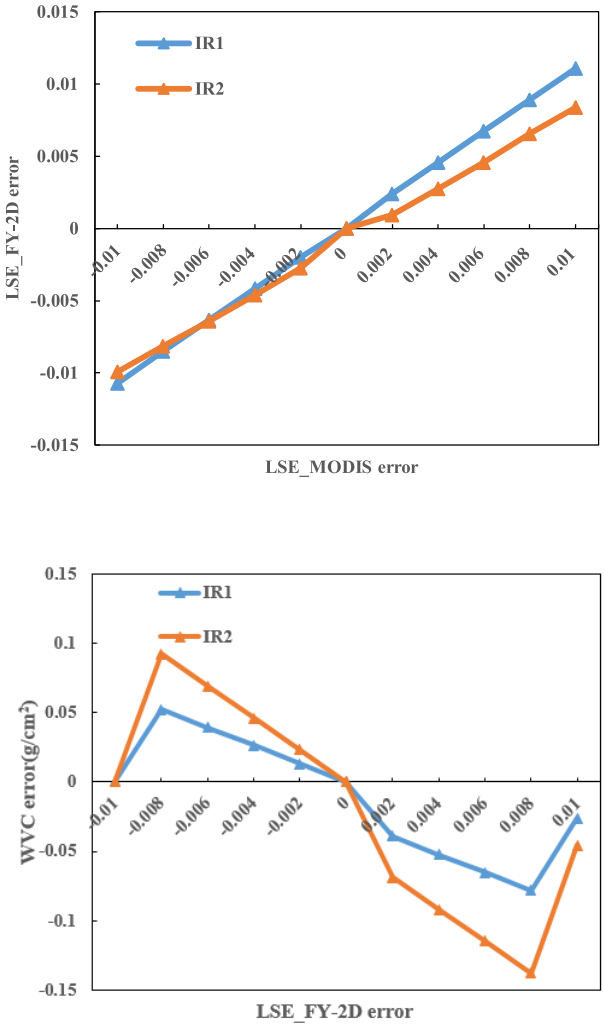

FIGURE 4. Sensitivity analysis of LSE and WVC.

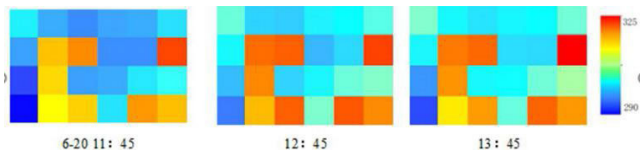

FIGURE 5. LST retrieval at 11:45, 12:45 and 13:45 (Beijing time) for 6.20, 2012.

B. LST ESTIMATION USING FY-2D

The LST was retrieved from June 20, 2012 to July 20, 2012. Figure 5 showed an example of retrieved LST in June 20, 2012. There is a relatively low value of LST in the oasis, located in the middle of study area. Meanwhile, the high value LST appeared in the region (non-vegetated desert region) around the oasis. The distribution of the retrieved LST is in accordance with that of oasis and desert. The low LST was observed in the oasis region (the middle part of Figure 4), the high LST was observed in the desert region (surrounding part of oasis).

C. VALIDATION OF LST ESTIMATION

In the study area, the retrieved LST was validated by the ground measured LST at the four selected sites, namely crop, wetland, desert 1 and desert 2 site, in Figure 6 and Table 2. In general, the basis, RMSE and R^2 were -3.48 K – 2.61 K, 2.86 K – 6.21 K and 0.53 - 0.67, respectively. In details, a more satisfactory accuracy of retrieved LST appeared at the two vegetated sites (crop and wetland sites) with RMSE of about 2.8 K. By contrast, there is a relatively lower accuracy of retrieved LST at the two non-vegetated sites (two desert sites) with RMSE of about 6.0 K. Obviously, even though that the refined split-window algorithm has improved the performance in the arid region, the LST still did not have a satisfactory accuracy in the non-vegetated regions.

D. COMPARISON WITH THE LST ESTIMATION WITH MODIS LST

Considered that the refined split-window algorithm is the official algorithm of MODIS LST product, the retrieved LST

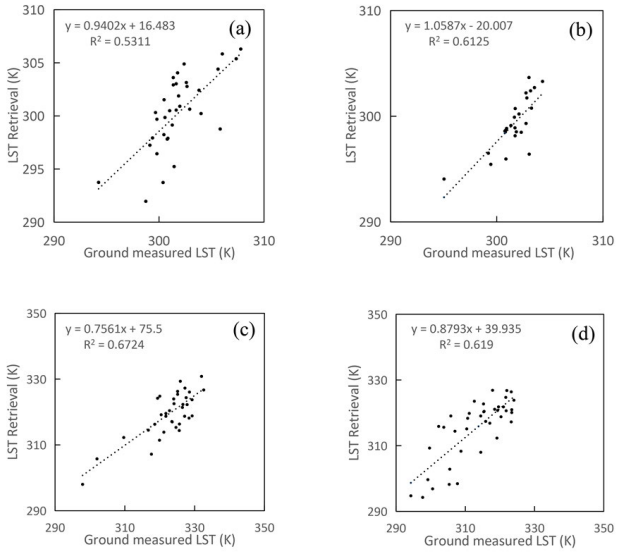

FIGURE 6. Relationship between ground-measured and FY-2D-derived LST at 4 sites: (a) crop site, (b) wetland site, (c) desert site1 and (d) desert site2.

TABLE 2. Comparison between ground-measured and FY-2D-derived LST.

Sites	Bias (K)	RMSE (K)	R^2
Crop	-1.40	2.86	0.53
Wetland	-2.31	2.77	0.61
Desert 1	-3.48	5.71	0.67
Desert 2	2.16	6.21	0.62

was compared with the MOD11 LST in the study region. Eleven MOD11 LSTs were selected due to their availability under clear sky during June 20 – July 20, 2012. The figure 7 showed the relationship of the retrieved LST and MOD11 LST at all 4 sites. The MODIS LST pixels were averaged within a window size of 5 × 5 to match with the spatial resolution of FY-2D. The R^2 is 0.83 with the bias (−0.4K) and RMSE (2.75K), respectively. The retrieved LST was in a relatively good accordance with the MOD11 LST.

Figure 8 revealed the spatial distribution of the differences between FY-2D-derived LST and MODIS LST product. At the most of the moments, the underestimation appeared in the oasis region (the middle part of the study area), and an overestimation appeared in the desert region (around the oasis). The amount of pixels with deference of less than ± 2 K accounted for about 40% of the total (Figure 9). And the amount of pixels with difference of more than ± 6 K accounted for less than 20% of the total.

V. DISCUSSION

In general, the coefficient of the refined split-window algorithm was calibrated to match with FY-2D initially. The algorithm can be used to retrieve LST and get a relatively accuracy in the arid region, especially in the vegetated region. However, the ability of the algorithm for FY-2D still seems to be improved in the desert region, even though the algorithm has

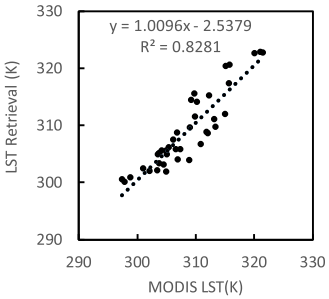

FIGURE 7. Relationship between MODIS and FY-2D-derived LST at all 4 sites.

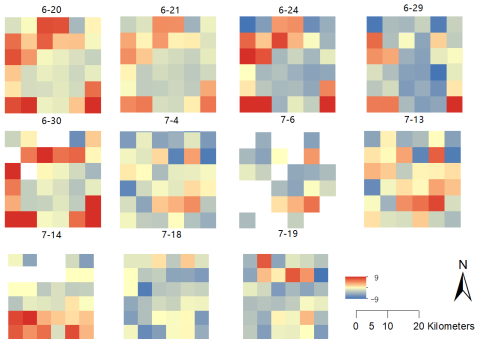

FIGURE 8. Differences between FY-2D-derived LST and MODIS LST.

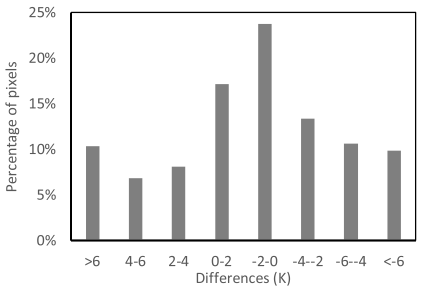

FIGURE 9. The percentage of Differences between FY-2D-derived LST and MODIS LST.4.

improved the performance in the sandy region [7]. The similar performance of the proposed coefficients was also studied for the other Fengyun sensors, for example FY-2C, FY-2E and FY-4A [38] The relatively unsatisfactory performance in the desert region was also reported in those studies [38]. Although the performance of the proposed coefficients was not so good because of the limitation of the quality of the sensors, the goal of this study is to make use of the old sensors and to try the best to get a relatively accurate performance.

Besides the limitation of the algorithm, there are several reasons why there are discrepancies between the FY-2D retrieved and MOD 11 LST. Firstly, the spatial resolution of them are significantly different (FY-2D, 5km vs MOD11 1km). The heterogeneity of the pixel with low resolution is obviously larger than that with high resolution, and it affect possibly reliability of cross validation. Secondly, they are not temporally matched exactly in the same moment. The

discrepancy of the imaging moment can be up to 30 minutes, and the difference of FY LST and MOD 11 LST can be more than 10 K in extreme cases [39]. Thirdly, the weak signal-to-noise ratio of the FY-2D data could also cause significant discrepancies between FY-2D-derived and MODIS LSTs [20], [22].

In the future, to improve the accuracy of LST retrieval using FY-2D data, there are some potential approaches that can be made use of: (1) the component LST retrieval or the spatial downscaling of LST can be used to eliminate the influence of the heterogeneity on accuracy of LST [29], [40], [41], [42], [43]. (2)The temporal-effect normalization model or the approach of temporal component decomposition can be introduced to match the imaging time of FY-2D with that of MODIS [44], [45]. (3) The more reliable land surface emissivity can be derived from other kind of sensors to retrieve LST considered about the less dramatic variation of emissivity during a period [31], [46]. It is believed that those further improvements can boost the performance of our algorithm for FY-2D in the future study.

VI. CONCLUSION

As the official algorithm of MODIS LST product, the refined split-window algorithm was used to retrieve LST by MODIS and was excepted to improve its performance in the arid desert regions. To explore the applicability of that algorithm for FY-2D, this paper initially simulated and calibrated the coefficient of the refined split-window algorithm for FY-2D. Specially, LSE in the two thermal infrared channels (IR1, 10.3-11.3 μm and IR2, 11.5-12.5 μm) is estimated from the LSE in channels 31 and 32 of the MODIS product. In addition, the FY-2D LSE was derived from MODIS LSE based on the linear fitting of the two thermal infrared channels between FY-2D and MODIS.

Then the LST was retrieved and validated in the arid region. Visually, the spatial pattern of retrieval was similar to that of oasis and desert. At the ground sites, the retrieved LST showed a relatively satisfactory accuracy with the RMSE and R^2 were 2.86 K – 6.21 K and 0.53 - 0.67, respectively. A higher (lower) accuracy of retrieval was observed at the vegetated (non-vegetated) sites with RMSE of 2.8K (6.0K). In addition, the retrieval was also compared with the MOD11, and revealed the general similarity between them with the R^2 of 0.83. There are about 40% of all pixel where less than $\pm$2 K difference was observed. In addition, there is only less than 20% of all pixels where more than $\pm$ 6 K difference was existed. This paper is helpful to the exploration of the ability of refined split-window algorithm for Chinese Geostationary Meteorological Satellite and the production of hourly LST datasets.

ACKNOWLEDGMENT

The authors thank the Cold and Arid Regions Science Data Center at Lanzhou for providing observation data (http://westdc.westgis.ac.cn). They also thank Prof. S. M. Liu and Dr. Z. W. Xu for their kind assistance in providing field data and help in field visit. They also thank Prof. J. Zhou and Dr. J. Ma for their comments and supports. Besides, they also thank the anonymous referees for their insightful comments and suggestions.

REFERENCES

[1] X. Pan, Y. Liu, and X. Fan, "Comparative assessment of satellite-retrieved surface net radiation: An examination on CERES and SRB datasets in China," *Remote Sens.*, vol. 7, no. 4, pp. 4899–4918, 2015, doi: 10.3390/rs70404899.

[2] X. Pan, Y. Liu, G. Gan, X. Fan, and Y. Yang, "Estimation of evapotranspiration using a nonparametric approach under all sky: Accuracy evaluation and error analysis," *IEEE J. Sel. Topics Appl. Earth Observ. Remote Sens.*, vol. 10, no. 6, pp. 2528–2539, Jun. 2017, doi: 10.1109/JSTARS.2017.2707586.

[3] J. Hu, Y. Yang, X. Pan, Q. Zhu, W. Zhan, Y. Wang, W. Ma, and W. Su, "Analysis of the spatial and temporal variations of Land Surface Temperature based on local climate zones: A case study in Nanjing, China," *IEEE J. Sel. Topics Appl. Earth Observ. Remote Sens.*, vol. 12, no. 11, pp. 4213–4223, Nov. 2019, doi: 10.1109/JSTARS.2019.2926502.

[4] M. Chen, X. Jiang, H. Wu, Y. Qian, and N. Wang, "Temperature and emissivity retrieval from low-emissivity materials using hyperspectral thermal infrared data," *Int. J. Remote Sens.*, vol. 40, nos. 5–6, pp. 1655–1671, Mar. 2019.

[5] F.-C. Zhou, Z.-L. Li, H. Wu, S.-B. Duan, X. Song, and G. Yan, "A remote sensing method for retrieving land surface emissivity and temperature in cloudy areas: A case study over South China," *Int. J. Remote Sens.*, vol. 40, nos. 5–6, pp. 1724–1735, Mar. 2019.

[6] Z. Wan and J. Dozier, "A generalized split-window algorithm for retrieving Land-Surface Temperature from space," *IEEE Trans. Geosci. Remote Sens.*, vol. 34, no. 4, pp. 892–905, Jul. 1996, doi: 10.1109/36.508406.

[7] Z. Wan, "Z new refinements and validation of the collection-6 MODIS land-surface temperature/emissivity product," *Remote Sens. Environ.*, vol. 140, pp. 36–45, Jan. 2014, doi: 10.1016/j.rse.2013.08.027.

[8] C. J. Jiménez-Muoz and J. A. Sobrino, "A generalized single-channel method for retrieving land surface temperature from remote sensing data," *J. Geophys. Res. Atmos.*, vol. 108, no. D8, Nov. 2003, Art. no. D08112.

[9] L. M. Mcmillin, "Estimation of sea surface temperatures from two infrared window measurements with different absorption," *J. Geophys. Res.*, vol. 80, no. 36, pp. 5113–5117, Dec. 1975, doi: 10.1029/JC080i036p05113.

[10] B.-H. Tang, "Nonlinear split-window algorithms for estimating land and sea surface temperatures from simulated Chinese Gaofen-5 satellite data," *IEEE Trans. Geosci. Remote Sens.*, vol. 56, no. 11, pp. 6280–6289, Nov. 2018, doi: 10.1109/TGRS.2018.2833859.

[11] T. Liu and G. Yan, "Retrieval of global orbit drift corrected Land Surface Temperature from long-term AVHRR data," *Remote Sens.*, vol. 11, no. 23, p. 2843, Nov. 2019, doi: 10.3390/rs11232843.

[12] J. Ma, J. Zhou, F.-M. Göttsche, S. Liang, S. Wang, and M. Li, "A global long-term (1981–2000) Land Surface Temperature product for NOAA AVHRR," *Earth Syst. Sci. Data*, vol. 12, no. 4, pp. 3247–3268, Dec. 2020, doi: 10.5194/essd-12-3247-2020.

[13] Y. Shu, S. Stisen, K. H. Jensen, and I. Sandholt, "Estimation of regional evapotranspiration over the north China plain using geostationary satellite data," *Int. J. Appl. Earth Observ. Geoinf.*, vol. 13, no. 2, pp. 192–206, Apr. 2011, doi: 10.1016/j.jag.2010.11.002.

[14] D. Sun and R. T. Pinker, "Estimation of land surface temperature from a Geostationary Operational Environmental Satellite (GOES-8)," *J. Geophys. Res., Atmos.*, vol. 108, no. D11, p. 4326, Jun. 2003, doi: 10.1029/2002jd002422.

[15] G.-M. Jiang and R. Liu, "Retrieval of sea and Land Surface Temperature from SVISSR/FY-2C/D/E measurements," *IEEE Trans. Geosci. Remote Sens.*, vol. 52, no. 10, pp. 6132–6140, Oct. 2014, doi: 10.1109/TGRS.2013.2295260.

[16] Y. Hu, L. Zhong, Y. Ma, M. Zou, K. Xu, Z. Huang, and L. Feng, "Estimation of the Land Surface Temperature over the Tibetan Plateau by using Chinese FY-2C geostationary satellite data," *Sensors*, vol. 18, no. 2, p. 376, Jan. 2018, doi: 10.3390/s18020376.

[17] R. Li, H. Li, L. Sun, Y. Yang, T. Hu, Z. Bian, B. Cao, Y. Du, and Q. Liu, "An operational split-window algorithm for retrieving Land Surface Temperature from geostationary satellite data: A case study on Himawari-8 AHI data," *Remote Sens.*, vol. 12, no. 16, p. 2613, Aug. 2020, doi: 10.3390/rs12162613.

[18] H. Fang, "Retrieval of land surface parameters from geostationary satellite data: An overview of recent developments," (in Chinese), *Nat. Remote Sens. Bull.*, vol. 25, no. 1, pp. 109–125, 2021.

[19] B. Tang, Y. Bi, Z.-L. Li, and J. Xia, "Generalized split-window algorithm for estimate of Land Surface Temperature from Chinese geostationary FengYun meteorological satellite (FY-2C) data," *Sensors*, vol. 8, no. 2, pp. 933–951, Feb. 2008, doi: 10.3390/s8020933.

[20] X. Zhang and J. Wang, "Estimation of Land Surface Temperature using geostationary meteorological satellite data," *Remote Sens. Technol. Appl.*, vol. 28, no. 1, pp. 12–17, 2013.

[21] X. Song, Y. Wang, B. Tang, P. Leng, S. Chuan, J. Peng, and A. Loew, "Estimation of Land Surface Temperature using FengYun-2E (FY-2E) data: A case study of the source area of the yellow river," *IEEE J. Sel. Topics Appl. Earth Observ. Remote Sens.*, vol. 10, no. 8, pp. 3744–3751, Aug. 2017, doi: 10.1109/JSTARS.2017.2682961.

[22] X. Pan, Y. Liu, X. Fan, and G. Gan, "Two energy balance closure approaches: Applications and comparisons over an oasis-desert ecotone," *J. Arid Land*, vol. 9, pp. 51–64, Feb. 2017, doi: 10.1007/s40333-016-0063-2.

[23] X. Cheng, G. Liu, S. Xiao, Q. Ma, M. Jin, R. Che, T. Liu, Q. Wang, W. Qi, Y. Wen, J. G. Li, H. Y. Zhu, G. F. Guo, J. W. Ran, Y. H. Wang, S. G. Zhu, Z. L. Zhou, J. Hu, X. L. Xu, and Z. W., "Heihe watershed allied telemetry experimental research (HiWATER): Scientific objectives and experimental design," *Bull. Amer. Meteorolog. Soc.*, vol. 94, no. 8, pp. 1145–1160, 2013, doi: 10.1175/BAMS-D-12-00154.1.

[24] H. Li and H. Wang, "HiWATER: ASTER LST and LSE dataset in the middle reaches of the Heihe River Basin (2012)," *Big Earth Data Platform Three Poles*, 2017, doi: 10.3972/hiwater.220.2015.db.

[25] Y. Pei, "Optical design for multichannel scanning radiometer on board FY-2 geostationary meteorological satellite," *Proc. SPIE*, vol. 4130, pp. 773–782, Dec. 2000, doi: 10.1117/12.409920.

[26] H. Han, N. Guo, D. Cai, and J. Wang, "FY-2D retrieved surface temperature change as a predictor for sandstorm forecasting over Northwest China," in *Proc. IEEE Int. Geosci. Remote Sens. Symp.*, Jul. 2011, pp. 3261–3264, doi: 10.1109/IGARSS.2011.6049915.

[27] G. Yang, R. Pu, C. Zhao, W. Huang, and J. Wang, "Estimation of subpixel Land Surface Temperature using an endmember index based technique: A case examination on ASTER and MODIS temperature products over a heterogeneous area," *Remote Sens. Environ.*, vol. 115, no. 5, pp. 1202–1219, May 2011, doi: 10.1016/j.rse.2011.01.004.

[28] Y. Yang, C. Cao, X. Pan, X. Li, and X. Zhu, "Downscaling Land Surface Temperature in an arid area by using multiple remote sensing indices with random forest regression," *Remote Sens.*, vol. 9, no. 8, p. 789, Jul. 2017, doi: 10.3390/rs9080789.

[29] A. Sekertekin and S. Bonafoni, "Sensitivity analysis and validation of daytime and nighttime Land Surface Temperature retrievals from Landsat 8 using different algorithms and emissivity models," *Remote Sens.*, vol. 12, no. 17, p. 2776, Aug. 2020, doi: 10.3390/rs12172776.

[30] K. Wang and S. Liang, "Evaluation of ASTER and MODIS Land Surface Temperature and emissivity products using long-term surface longwave radiation observations at SURFRAD sites," *Remote Sens. Environ.*, vol. 113, no. 7, pp. 1556–1565, Jul. 2009, doi: 10.1016/j.rse.2009.03.009.

[31] F. Becker and Z. Li, "Surface temperature and emissivity at various scales: Definition, measurement and related problems," *Remote Sens. Rev.*, vol. 12, nos. 3–4, pp. 225–253, Jan. 1995, doi: 10.1080/02757259509532286.

[32] B. Tang and Z.-L. Li, "Estimation of instantaneous net surface longwave radiation from MODIS cloud-free data," *Remote Sens. Environ.*, vol. 112, no. 9, pp. 3482–3492, Sep. 2008, doi: 10.1016/j.rse.2008.04.004.

[33] W. Zhengming and J. Dozier, "Land-surface temperature measurement from space: Physical principles and inverse modeling," *IEEE Trans. Geosci. Remote Sens.*, vol. 27, no. 3, pp. 268–278, May 1989, doi: 10.1109/36.17668.

[34] Z.-L. Li, L. Jia, Z. Su, Z. Wan, and R. Zhang, "A new approach for retrieving precipitable water from ATSR2 split-window channel data over land area," *Int. J. Remote Sens.*, vol. 24, no. 24, pp. 5095–5117, Jan. 2003, doi: 10.1080/0143116031000096014.

[35] F. Wang, Z. Qin, C. Song, L. Tu, A. Karnieli, and S. Zhao, "An improved mono-window algorithm for Land Surface Temperature retrieval from Landsat 8 thermal infrared sensor data," *Remote Sens.*, vol. 7, no. 4, pp. 4268–4289, Apr. 2015, doi: 10.3390/rs70404268.

[36] L. Wang, Y. Lu, and Y. Yao, "Comparison of three algorithms for the retrieval of Land Surface Temperature from Landsat 8 images," *Sensors*, vol. 19, no. 22, p. 5049, Nov. 2019, doi: 10.3390/s19225049.

[37] J. Fan, Q. Han, S. Wang, H. Liu, L. Chen, S. Tan, H. Song, and W. Li, "Evaluation of Fengyun-4A detection accuracy: A case study of the Land Surface Temperature product for Hunan province, central China," *Atmosphere*, vol. 13, no. 12, p. 1953, Nov. 2022, doi: 10.3390/atmos13121953.

[38] A. H. Y. B. X. Y. Wang and X. J. D. Hu, "Research on Land Surface Temperature downscaling method based on diurnal temperature cycle model deviation coefficient calculation," *Nat. Remote Sens. Bull.*, vol. 25, no. 8, pp. 1735–1748, 2021, doi: 10.11834/jrs.20211181.

[39] X. Pan, X. Zhu, Y. Yang, C. Cao, X. Zhang, and L. Shan, "Applicability of downscaling Land Surface Temperature by using normalized difference sand index," *Sci. Rep.*, vol. 8, no. 1, p. 9530, Jun. 2018, doi: 10.1038/s41598-018-27905-0.

[40] Y. Chen, Y. Yang, X. Pan, X. Meng, and J. Hu, "Spatiotemporal fusion network for Land Surface Temperature based on a conditional variational autoencoder," *IEEE Trans. Geosci. Remote Sens.*, vol. 60, 2022, Art. no. 5002813, doi: 10.1109/TGRS.2022.3183114.

[41] Y. Shi, "Thermal infrared inverse model for component temperatures of mixed pixels," *Int. J. Remote Sens.*, vol. 32, no. 8, pp. 2297–2309, Mar. 2011, doi: 10.1080/01431161003698252.

[42] Z. Bian, Q. Xiao, B. Cao, Y. Du, H. Li, H. Wang, Q. Liu, and Q. Liu, "Retrieval of leaf, sunlit soil, and shaded soil component temperatures using airborne thermal infrared multiangle observations," *IEEE Trans. Geosci. Remote Sens.*, vol. 54, no. 8, pp. 4660–4671, Aug. 2016, doi: 10.1109/TGRS.2016.2547961.

[43] P. Hu, A. Wang, Y. Yang, X. Pan, X. Hu, Y. Chen, X. Kong, Y. Bao, X. Meng, and Y. Dai, "Spatiotemporal downscaling method of Land Surface Temperature based on daily change model of temperature," *IEEE J. Sel. Topics Appl. Earth Observ. Remote Sens.*, vol. 15, pp. 8360–8377, 2022, doi: 10.1109/JSTARS.2022.3209012.

[44] X. Zhang, J. Zhou, F.-M. Gottsche, W. Zhan, S. Liu, and R. Cao, "A method based on temporal component decomposition for estimating 1-km all-weather Land Surface Temperature by merging satellite thermal infrared and passive microwave observations," *IEEE Trans. Geosci. Remote Sens.*, vol. 57, no. 7, pp. 4670–4691, Jul. 2019, doi: 10.1109/TGRS.2019.2892417.

[45] L. F. Chen, Z.-L. Li, Q. H. Liu, S. Chen, Y. Tang, and B. Zhong, "Definition of component effective emissivity for heterogeneous and non-isothermal surfaces and its approximate calculation," *Int. J. Remote Sens.*, vol. 25, no. 1, pp. 231–244, Jan. 2004, doi: 10.1080/0143116031000116426.

[46] H. Ren, R. Liu, and Q. Qin, "Mapping finer-resolution land surface emissivity using Landsat images in China," *J. Geophys. Res.*, vol. 122, no. 13, pp. 6764–6781, 2017, doi: 10.1002/2017JD026910.

XIN PAN received the B.S. degree in surveying and mapping from Wuhan University, Wuhan, China, in 2011, the M.S. degree in surveying and mapping from Hohai University, Nanjing, China, in 2013, and the Ph.D. degree in cartography and geographical information system from the Nanjing Institute of Geography and Limnology, Chinese Academy of Sciences, Nanjing, in 2016.

He is currently an Associate Professor with the School of Earth Science and Engineering, Hohai University. His research interests include the remote sensing retrieval and validation of land surface evapotranspiration and land surface temperature.

SUYI LIU received the B.S. degree in geomatics from Southwest Petroleum University, Chengdu, China, in 2021. She is currently pursuing the degree in surveying and mapping with the School of Earth Science and Engineering, Hohai University.

She is mainly engaged in quantitative remote sensing-related research.

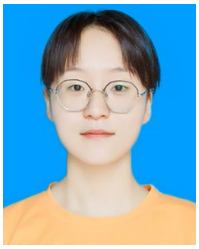

ZI YANG received the B.S. degree in remote sensing science and technology from Henan Polytechnic University, Jiaozuo, China, in 2020, and the M.S. degree in surveying and mapping engineering from Hohai University, Nanjing, China, in 2022, where she is currently pursuing the Ph.D. degree in surveying and mapping science and technology.

Her main research interest includes quantitative remote sensing retrieval.

XI ZHU received the bachelor's degree in surveying and mapping and the master's degree in remote sensing and photogrammetry from Hohai University, Nanjing, China, in 2016 and 2019, respectively.

His research interests include thermal infrared remote sensing and ground temperature.

YINGBAO YANG received the Ph.D. degree in cartography and geographical information system from the Nanjing Institute of Geography and Limnology, Chinese Academy of Sciences, Nanjing, China, in 2005.

She is currently a Professor with the School of Earth Science and Engineering, Hohai University. Her research interests include the remote sensing retrieval of land surface temperature and the analysis of urban thermal environments.

WENYING XIE received the bachelor's degree in surveying and mapping from Jining University, Jining, China, in 2021. She is currently pursuing the master's degree in surveying and mapping science and technology (photogrammetry and remote sensing) with Hohai University.

Her research interest includes quantitative remote sensing.

JIE YUAN received the B.S. degree in marine technology from Shanghai Ocean University, Shanghai, China, in 2022. She is currently pursuing the degree in surveying and mapping with the School of Earth Science and Engineering, Hohai University.

Her research interest includes hydrological remote sensing.

ZHANCHUAN WANG received the bachelor's degree in geographic information science from the Nanjing University of Posts and Telecommunications, Nanjing, China, in 2022. He is currently pursuing the degree in surveying and mapping science and technology with the School of Earth Science and Engineering, Hohai University.

HAO SONG received the bachelor's degree in surveying and mapping from Xuchang University, Xuchang, China, in 2022. He is currently pursuing the master's degree with the School of Earth Science and Engineering, Hohai University.

His research interest includes remote sensing object extraction.